ELSEVIER

Contents lists available at ScienceDirect

International Journal of Biological Macromolecules

journal homepage: www.elsevier.com/locate/ijbiomac



The novel *Craymin* gene regulates calcium carbonate crystallization in the crustacean exoskeleton[★]

Shai A. Shaked ^{a,b}, Rivka Manor ^{a,b}, Simy Weil ^{a,b}, Idan Pery ^a, Eliahu D. Aflalo ^{a,b,c}, Sana Huleihel ^d, Nitzan Maman ^d, Lonia Friedlander ^d, Amir Sagi ^{a,b,*}

- ^a Department of Life Sciences, Ben-Gurion University of the Negev, Beer-Sheva, Israel
- ^b The National Institute for Biotechnology in the Negev, Ben-Gurion University of the Negev, Beer-Sheva, Israel
- ^c Department of Life Sciences, Achva Academic College, Israel
- ^d Ilse Katz Institute for Nanoscale Science & Technology, Ben-Gurion University of the Negev, Beer-Sheva, Israel

ARTICLE INFO

Keywords: Biomineralization encoding gene Crustaceans Exoskeletal CaCO₃

ABSTRACT

Crustaceans undergo periodic exoskeleton replacement during a rapid and highly regulated molt cycle to allow growth and/or morphological changes. The new exoskeleton is hardened in a biomineralization process involving various minerals, mainly amorphous calcium carbonate and calcite, its main crystalline polymorph. Biomineralization also requires the involvement of proteins, but knowledge of the protein-encoding genes in crustaceans remains scarce. To address this knowledge gap, we utilized binary expression pattern analysis of a molt-related transcriptomic library generated from the cuticle-forming epithelium of the crayfish Cherax quadricarinatus. We thereby mined a gene encoding a glycine-rich protein that was found to exhibit exoskeletonmineralization-related molt expression; we named this gene Craymin (crayfish mineralization). The Craymin protein was found in the exoskeleton cuticle and in exuvia, and RNA interference knockdown of its encoding gene reduced its relative expression in epithelium-forming cells by 90 %. Following knockdown, newly formed cuticles were largely depleted of Craymin protein molecules, resulting in a 47 % reduction in exoskeleton calcium content, together with larger CaCO3 crystallites, compared to the control. Concomitantly with the reduction in calcium content, more than 80 % reduction in confined high-density regions (representing highly mineralized cuticular areas) was measured following knockdown, resulting in an overall reduction of cuticular density. These alterations were phenotypically translated into a 50 % reduction in cuticular width, accompanied by decreased structural integrity. Craymin thus seems to be a key protein in the crustacean exoskeleton, being involved in cuticular mineralization by mediating the deposition of calcium and the control of its crystalline polymorphs.

1. Introduction

As long as three decades ago, Lowenstam and Weiner described crustaceans as the 'champions of mineral mobilization and deposition in the animal kingdom' [1]. Since that time, significant research has been devoted to the ways in which the crustacean exoskeleton is formed and mineralized [2–10]. Much of that research was conducted on crayfish species, which are regarded as particularly suitable species for the study of protein-encoding genes related to mineralization processes [11–15]. The utility of crayfish as model species is due largely to the availability of a well-established marker – the molt mineralization index (MMI; gastrolith width /carapace length) – that can be used to monitor the molt

cycle precisely, easily and non-invasively [16]. Paradoxically, however, there are very few reports of crayfish genes encoding proteins known to be directly involved in or to govern biomineral crystallization [10,17], with most of the work on the subject being reported for mussels and scallops [18–22].

Previous work has indicated that the formation of the crustacean exoskeleton involves different forms of calcium carbonate (amorphous or crystalline polymorphs) [15,16,23–25] and that biomineral crystallization can be directed in a time- and location-dependent manner [16]. Calcium distribution across $\it C. quadricarinatus$ cuticle was found to be heterogenous with calcium concentration ranging between 0 and 60 % at some points (personal connection, unpublished data). Proper

^{*} This article is part of a Special issue entitled: 'Nucleic Acids in Crustaceans' published in International Journal of Biological Macromolecules.

^{*} Corresponding author at: Department of Life Sciences, Ben-Gurion University of the Negev, Beer-Sheva, Israel. *E-mail address*: sagia@bgu.ac.il (A. Sagi).

exoskeletal properties and functions in crustaceans depend on precise control of the biomineral polymorphs that form the hardened shell essential for supporting muscle movements and providing protection from predators [15,26]. While a small number of protein-encoding genes responsible for exoskeleton scaffold formation are already known in crustaceans [27,28], it is believed that there are many more functional protein-encoding genes that act in concert in the biomineralization process [29]. Examples from other biomineralizing organisms suggest that proteins with acidic moieties are required for the initiation of mineralization (i.e., mineral nucleation and sedimentation) [30-34]. On the basis of some known examples from mussels, scallops and even mineralizing bacteria, it has been suggested that - among such proteins relatively short (around 150AA) glycine-rich proteins play a key role in biomineralization [20,35–38]. Nonetheless, while much is known about crustacean exoskeleton mineral composition and polymorphs [4,9,39-42], the genetically encoded proteinaceous toolkit involved in controlling biomineralization and directing biomineral crystallization is yet to be deciphered in its entirety. Some information regarding proteins with possible involvement in the process of biomineralization is available for a small number of invertebrates [2,43-49]; these proteins all exhibit the common feature of glycine-rich regions [20,38,45]. Indeed, functional genomics and in-vitro crystallization experiments have shown that glycine-containing proteins, more specifically proteins with glycine repeats (G-G-X or G-X), affect CaCO3 biomineralization [38,50,51], although to date there are no studies demonstrating that such proteins interact directly with calcium compounds.

With an ultimate aim to reveal the genetic and molecular toolkit of crustacean exoskeleton mineralization and the immediate aim to search for novel candidate protein-encoding genes involved in exoskeleton hardening, we focused on the redclaw crayfish *Cherax quadricarinatus* as a model crustacean species. The current study leverages previous work performed in our laboratory, namely, the development of binary expression pattern analysis, the generation of a wide molt-related transcriptomic database [29,52], and an experimental protocol based on molt induction, followed by noninvasive tracking of molt progress [16] by monitoring the MMI over the molt cycle [16].

Beyond the basic need to understand how crustaceans control the function of biominerals through prevention or promotion of crystallization [15,26,53], interest in exoskeleton biomimesis for diverse applications is on the rise [54–56]. Mining and characterizing a novel protein-encoding gene involved in *C. quadricarinatus* exoskeleton mineralization will contribute to revealing the entire intricate mechanism controlling the functioning of CaCO₃ polymorphs.

2. Materials and methods

2.1. Animals and molt induction

C. quadricarinatus crayfish were grown in and collected from artificial ponds as previously described [53]. For molt induction experiments, inter-molt crayfish were held in individual cages and endocrinologically induced to enter pre-molt through daily injections of α -ecdysone (Sigma-Aldrich) for 10 days [52]. Molt cycle progression of each animal was monitored daily by X-raying the gastrolith and then determining the MMI, which is known to correlate with molt stage and hormonal levels [16]. Post-molt animals were harvested on the day following ecdysis. For all dissections, crayfish were first anesthetized on ice for 10–15 min.

2.2. In-silico mining and characterization of mineralization-proteinencoding genes

To mine and characterize mineralization-protein-encoding genes, the binary expression pattern [52] was utilized on the molt-related transcriptomic library described before [29]. This method subjects each candidate transcript to a four-digit code, representing relative expression level at each of the molt stages, whereas '0' and '1' denote

relatively low and high expression levels, respectively, requiring a significant statistical difference between the two. Transcripts exhibiting a binary expression pattern of 0001 at the molt-related transcriptomic library, which indicated high expression concomitant with post-molt cuticle mineralization, were selected as candidate transcripts and compiled into a list. The list was filtered such that it retained only relatively short protein-encoding genes (~ 500 bp open reading frames (ORFs)), with GGX-encoding repeats, suggesting their function as mineralization-related protein-encoding genes. The selected candidate transcripts were then computationally translated into proteins using the Translate Tool from the ExPASy Proteomics Server [57]. Mined candidate proteins were examined against the molt-related transcriptomic library [29] to find possible paralogues by using TBLASTX [58]. Predicted protein sequences were then analyzed using various bioinformatics tools. First, the amino acid content and predicted pI of each protein were calculated using the ProtParam tool (http://web.expasy. org/protparam/). Thereafter, to find sequence similarities, multiple sequence alignment (MSA) was conducted with Clustal Omega [59]. Intrinsically disordered regions and α -helices in the active protein were predicted with the XtalPred web server [60]. In summary, by implementation of binary expression pattern analysis on our molt-related transcriptomic library, a new protein-encoding gene with putative mineralization properties was mined. This gene, which we designated Craymin (crayfish mineralization), was subsequently found to encode a small (~17 kDa) glycine-rich protein (see below).

2.3. 3' and 5' rapid amplification of cDNA ends (RACE)

To reveal the full ORF of the *Craymin* protein-encoding gene in cuticle-forming epithelium, 3′ and 5′ RACE were carried out using the SMARTER RACE kit (Takara Bio, Mountain View, CA, USA). RNA from cuticle-forming epithelium obtained post-molt was transcribed according to the SMARTER RACE kit protocol. Primers for 3′ and 5′ RACE were designed using the Primer3 tool [61] and are listed in Table S1. PCR product size was determined in 1.5 % agarose gel. The PCR product was then cleaned using Nucleospin gel and PCR cleanup columns (Machery-Nagel, Düren, Germany), cloned, and sequenced. Sequences were analyzed using Sequencher software (Gene Codes Corporation, Ann Arbor, MI, USA) to determine sequencing quality, resulting in delineation of the complete ORF of the *Craymin* gene.

2.4. Craymin glycosylation and phosphorylation prediction

The Craymin protein sequence was analyzed to determine any putative glycosylated and phosphorylated amino acid residues. Glycosylation and phosphorylation predictions were performed using the NetNGlyc 1.0 tool [62] and the NetPhos 3.1 tool [63], respectively.

2.5. Craymin spatial-temporal expression

The Craymin spatial-temporal expression pattern was examined by RT-PCR, as follows. Molting was induced in 24C. quadricarinatus males, and six animals were then dissected at each of the four main molt stages (inter-molt, early pre-molt, late pre-molt, and post-molt). Total RNA was isolated from the carapace cuticle-forming epithelium, mandibleforming epithelium, eye-forming epithelium, hepatopancreas and abdominal muscle of the animals at the four main molt stages by using an EZ-RNA Total RNA Isolation Kit (Biological Industries, Beit Haemek, Israel) according to the manufacturer's protocol. First-strand cDNA was synthesized by reverse transcription using the qScript cDNA Kit (Quanta BioSciences, Gaithersburg, MD, USA) with 1 μg of total RNA. The specific primers used for PCR amplification are given in Table S1. PCR was performed with REDTaq ReadyMix PCR Reaction Mix (Sigma, St. Louis, MO, USA) under the following conditions: 94 °C for 2 min, followed by 40 cycles at 94 $^{\circ}$ C for 15 s, 55 $^{\circ}$ C for 30 s, 72 $^{\circ}$ C for 30 s, and 72 $^{\circ}$ C for 2 min. C. quadricarinatus 18S rRNA (accession no. AF235966) served as

the positive control.

2.6. In-vitro expression pattern validation using qPCR

RNA was extracted from the carapace cuticle-forming epithelium. In addition, for normalization, RNA was extracted from the muscle tissue of an inter-molt animal. First-strand cDNA was synthesized in a reverse transcriptase reaction. Relative quantification of transcript levels was performed using Roche Diagnostics FastStart Universal Probe Master Mix (Basel, Switzerland) and Roche Universal Probe Library probes. Probe #60 was used for Craymin qPCR. *C. quadricarinatus 18S rRNA*, which served as a normalizing gene, was also quantified by means of real-time RT PCR using the qcq18S F and qcq18S R primers with probe #74. All primer sequences are listed in Table S1. Reactions were performed with the ABI Prism7300 Sequence Detection System (Applied Biosystems, Foster City, CA, USA).

2.7. dsRNA production and silencing efficiency test

Craymin was silenced by RNA interference (RNAi) using dsRNA. For the production of dsRNA templates, two primer pairs, with a T7 overhang attached to one of them (forward or reverse) were planned using Primer3 [61]. Two PCR products were thus generated: the sense dsRNA strand of *Craymin* was generated with the primers Craymin dsRNA-F + T7 and Craymin dsRNA-R, while the anti-sense dsRNA strand was generated with the primers Craymin dsRNA-F and Craymin dsRNA-R + T7 (Table S1). Prior to molt induction, a total of 20C. quadricarinatus males at the intermolt stage (10 for treatment and 10 for control), each weighing 5-7 g, were injected once a week (for a total of two weeks) with Craymin dsRNA or crustacean saline [64], at a concentration of 5 μg dsRNA or saline per 1 g of body weight. Crustacean saline was used as a control, since it had previously been shown to be more suitable for this purpose than the dsRNA of an exogenous gene, such as GFP [65]. Thereafter, injections of dsRNA or saline were given every two days, concomitant with the daily injections of ecdysone. Molt stage was assessed every three days by X-ray imaging of the developing gastroliths and MMI calculations, as described above [16]. Total RNA extractions of the cuticle-forming epithelium were carried out one day post molt, and first-strand cDNA was used for relative quantification of Craymin expression levels by real-time PCR.

2.8. Cuticular mineralization phenotypic effects following Craymin knockdown

C. quadricarinatus males weighing 5–9 g were injected with dsRNA or crustacean saline together with ecdysone, as described above. Molt stage was determined in terms of the MMI prior to beginning the experiment, and only intermolt individuals were used. The cephalothorax section of the cuticle was subjected to protein extraction for assessment of knockdown efficiency at the protein level. Determination of phenotypic silencing effects on cuticle mineral content, distribution and structural integrity were performed on dried cuticular fragments.

2.9. Protein extraction from cuticles and exuviae

For quantitative determination of Craymin protein following the knockdown experiment, post molt cuticles from eight silenced and eight control animals were harvested, and proteins were extracted from sections of the cephalothorax region, as described before [15]. Total mass of 2.38 g of cuticle was pooled from eight control and eight treated individuals. Extractions in each category (control and treated cuticles) were pooled, flash frozen in liquid nitrogen, and kept at $-80\,^{\circ}\mathrm{C}$ until analyzed. Protein bands were separated on 4–20 % SurePAGE gels (GenScript) using MES running buffer and visualized using Coomassie brilliant blue. A standard curve for protein quantification was constructed with bovine serum albumin (BSA). For standard curve

construction, aliquots (0.5, 1, 2, and 3 μg) of BSA were separated on the same gel as that used for the analysis of the control and treated cuticle samples. Protein quantification was performed using the gel analysis function of ImageJ software [66].

To determine whether Craymin is also present in the discarded exoskeleton, namely, whether the Craymin protein is a structural constituent of the cuticle, proteins were extracted from 45 g control postmolt cuticles and exuviae. The total cuticle and the whole shed shell were used for these protein extractions. The same protocol as that described above for treated and control cuticles was applied, with a modification of manual separation of the exoskeletal scaffold layer from both the cuticle and the exuvia immediately after the first centrifugation of the tissue homogenates. Those fractions were then centrifuged to facilitate separation of the soluble proteins from the exoskeletal scaffold. Samples were then centrifuged at room temperature at $1000 \times g$ for 1 min, and the protein supernatants were separated on 4–20 % SurePAGE gels (GenScript) with the same running conditions as those described above.

2.10. Tandem mass spectrometry (MS/MS) of cuticular and exuviae proteins

Extraction of protein bands from the above-described protein gels, mass spectrometry, and data analysis were performed according to Shechter et al. [7]. The reduction, alkylation, and trypsinization steps of the protein bands cut from the gels and then analyzed by MS/MS were carried out as previously described [67]. Proteins were validated against the transcriptomic library and the C. quadricarinatus proteome from Uniprot (https://www.uniprot.org/taxonomy/27406); for this purpose, the Sequest algorithm search tool of Proteome Discoverer 1.2 software (Thermo Fisher Scientific, San Jose, CA, USA) was used with the following search parameters: proteolytic enzyme trypsin, maximum two missed cleavage sites, cysteine carbamidomethylation, methionine oxidation, and a maximum of 20 ppm or 0.02 Da error tolerance for full scan and MS/MS analysis, respectively. Protein identification criteria were defined as a minimal score of >100, a minimum of two peptides, and a false discovery rate (FDR) with a P-value <0.01, as described before [68].

2.11. Scanning electron microscopy (SEM) and energy dispersive spectroscopy (EDS)

Carapace cuticles extracted from five control (injected with saline) and five treated crayfish (injected with Craymin dsRNA) were air-dried in a desiccator for three days. Thereafter, cross sections of each cuticle were embedded in Epon, which was cured at 60 °C for 48 h. Each specimen was positioned with the cuticle parallel to the block to ensure that the cuticle cross-section would be vertical to the electron beam. To expose the sample surface, the bottoms of the blocks were trimmed with a razor blade, and to reveal the cuticle cross sections, excess resin was cut off the tops of the blocks with a UC Enuity ultramicrotome (Leica, Wetzlar, Germany) equipped with a diamond knife. The trimmed blocks were mounted on clamp-equipped holders, wrapped in carbon tape (excluding the polished top surface) and sputter-coated with a 10-nm layer of iridium. A Helios G4 UC (Thermo Fisher Scientific, San Jose, CA, USA) dual-beam microscope was used for surface imaging. After the region of interest (ROI) had been located (in a vertically oriented and non-damaged cuticle), SEM images were acquired under different conditions (i.e., voltage, current, working distance) to provide differential information on the cuticular layers. Elemental EDS maps were acquired using Xflash 6160 EDS detector (Bruker, MA, USA) on the same dualbeam microscope at 10 kV beam energy and 1.6 nA beam current for 30 min (to acquire sufficient data for reliable quantitative maps). Quantitative elemental maps were calculated for the relevant cuticular elements (calcium, phosphorus and carbon). Line scans were extracted from the acquired maps. Calcium-rich layers found in EDS were then

analyzed by X-ray diffractometry (XRD) to find the most abundant ${\rm CaCO_3}$ polymorph.

2.12. X-ray diffraction of cuticle samples

The same cuticular samples described above (both control and silenced) were air-dried and then left as such or processed further by either mounting in Epon or grinding to a fine powder. CaCO3 polymorphs in the samples were analyzed by XRD using a Panalytical EmpyreanIII Diffractometer with iCore/dCore automated optics attachments and a pixCEL 3D detector. The diffractometer was operated in transmission (unprocessed cuticle) and reflectance (Epon mounted or ground samples) modes at 45 mA and 40 kV using a Cu-Kα source. Initial transmission and reflectance measurements were used to determine the CaCO₃ polymorphs present in the control and silenced cuticles. To investigate changes in CaCO₃ distribution across the cuticle and possible changes in the polymorphs with depth through the layers of the cuticle, dried cuticle samples were embedded in Epon in an upright position (with the epicuticle layer facing up) and cured as described above. Sample surfaces were exposed using the same protocol as that performed for SEM. Background XRD spectra of pure Epon were acquired prior to the first exposure. Serial exposures (increasing the depth into the cuticle by 2 µm each time) were performed on both control and treated cuticle samples until the most prominent calcite peak observed in each serial XRD measurement started to decrease, meaning the detected calciumrich layer had already been crossed. These measurements were performed in the high-resolution (HR) symmetric reflectance XRD measurement geometry with a fixed irradiation area of 4 mm². All measurements were conducted in the 2q range of 10–60°. Analysis of the collected diffractograms was performed using HighScore advanced diffraction analysis software (version 5.1) [69]. Rietveld refinement of the cuticle depth profile results was performed to investigate changes in CaCO₃ concentration and crystallinity/crystallite size in each measured layer.

2.13. Cuticle micro-CT analysis

Three-dimensional scans of control and treated cuticles were performed using a Bruker SkyScan 1272 micro-CT (Bruker, MA, USA). Scans were collected at 40 kV and 80 μA with an image voxel size of 2.5 μm per side. The scans were reconstructed using NRecon (version 1.7.5.9, Bruker). Visual analysis was performed, and images were generated using StradView (https://mi.eng.cam.ac.uk/Main/StradView). Detection of high-density (X-ray transmission below transmission in air) and low-density (X-ray transmission equivalent to transmission in air) regions within the measured samples were performed on equivalent volumetric regions of interest (VOI) for the control and silenced samples by using CT Analyser (version 1.21.2.0, Bruker). The number of low-density (permeable to X-rays) regions surrounded by high-density (non-permeable to X-rays) barriers was counted, and the volume of the low-density regions and the surface areas of the surrounding barriers were calculated to reveal changes following *Craymin* knockdown.

2.14. Statistical analyses

For RT-qPCR, statistical analysis of relative transcription levels at the different molt stages was performed using one-way ANOVA followed by Tukey-HSD post hoc test. Prior to analysis, data were assessed for normality and homogeneity of variances. A logarithmic transformation was applied to meet the assumption of homogeneity of variances. Craymin silencing efficiency was assessed using Student's t-tests of independent groups. P < 0.05 was considered statistically significant in all statistical analyses performed.

3. Results

3.1. The Craymin protein-encoding gene

Craymin is a protein-encoding gene highly enriched in nucleotides encoding for glycine in a repetitive manner (Fig. 1a). Indeed, it was found that glycine comprises 25 % of Craymin protein amino acids (Table S2). In addition, the Craymin protein has a signal peptide and three consecutive low complexity regions (Fig. 1b). All these findings, together with a marked number of GGX repeats (Fig. 1c), suggest that Craymin is involved in $CaCO_3$ mineralization and crystallization. Craymin protein glycosylation and phosphorylation predictions suggest one glycosylation site (Supplementary Fig. S1a) and several phosphorylation sites per Craymin molecule (Fig. S1b).

3.2. Craymin transcription patterns in the exoskeleton-forming epithelium

The *Craymin* protein-encoding gene was found to be highly expressed at the post-molt mineralizing stage of *C. quadricarinatus* cuticular forming epithelia in silico, presenting a 0001 binary expression pattern (Fig. 2a), with significant statistical difference between high and low expression levels, as required (see materials and methods). Spatial-temporal transcription analysis confirmed this pattern, demonstrating the presence of *Craymin* in cuticle-forming epithelia (Fig. S2). Validation through RT-qPCR confirmed these *in-silico* and in-vitro observations and revealed a mineralization-related transcription of *Craymin* in the cuticle-forming epithelium, confirming the clear 0001 binary expression pattern described above (Fig. 2b). These findings supported further study of the *Craymin* protein-encoding gene as a mineralization-related candidate as a means to acquire a more comprehensive understanding of the mineralization process in the crayfish exoskeleton.

3.3. Structural association of Craymin with the exoskeletal scaffold

To validate the presence of Craymin in the exoskeleton, we specifically extracted proteins from exuviae and cuticle preparations as illustrated in Fig. S3a, aiming at extracting proteins associated with the exoskeletal scaffold. Profiles of proteins extracted from cuticles and exuviae of the chitinous skeletal scaffolds were found to contain Craymin (Fig. S3b, c). The protein bands representing Craymin from the cuticle and exuvia extractions were analyzed by MS/MS, revealing short peptides covering 35 % and 33 % of the full protein sequence, respectively. This analysis suggested that Craymin is indeed associated, either directly or through other proteins, with the chitinous structural scaffold (Fig. S3d).

3.4. Craymin knockdown efficiency at the RNA and protein levels

To study the role of Craymin in the mineralization of the *C. quadricarinatus* exoskeleton, we utilized temporal knockdown of *Craymin* via RNAi (i.e., dsRNA injections). RT-qPCR, performed to assess knockdown efficiency, revealed an approximately 90 % reduction in *Craymin* transcription levels compared to control (Fig. 3a). To assess the knockdown effect at the protein level, Craymin concentrations in control and treated animals were quantified by SDS-PAGE (using a BSA calibration curve) (Fig. S4). It was found that Craymin levels were significantly reduced following knockdown (Fig. 3b, c), as evidenced by almost invisible protein bands in the silenced samples (Fig. 3b) vs. clearly visible bands in the control samples (Fig. 3b, red ellipse). Those bands were validated as Craymin protein by MS/MS. A 60 % reduction in the Craymin protein level was found following knockdown via RNAi (Fig. 3c).

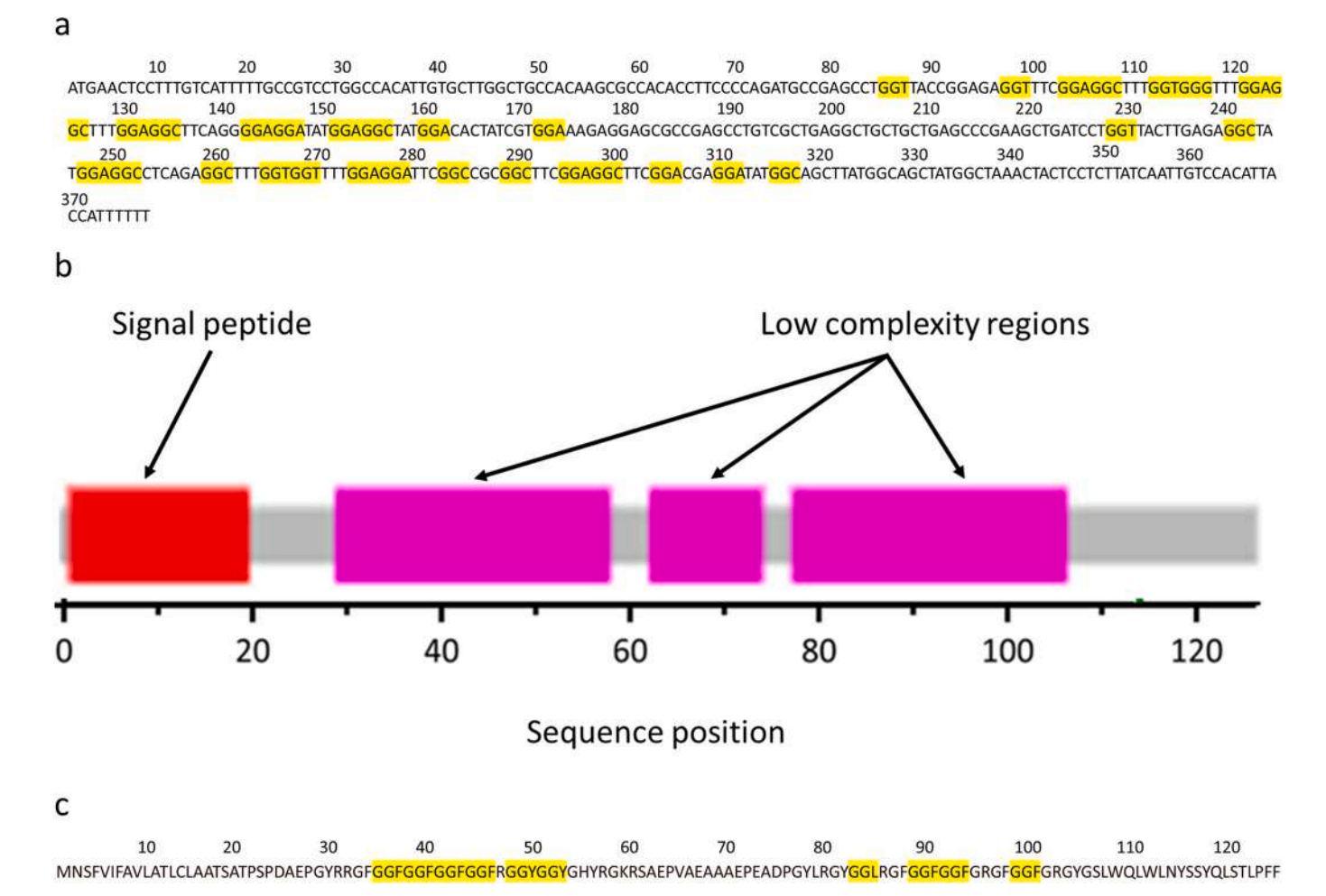


Fig. 1. Sequence characteristics of the *Craymin* protein-encoding gene. a) *Craymin* gene sequence with nucleotides encoding for glycine indicated in yellow. b) Schematic representation of the functional domains of the Craymin protein derived from SMART. c) Craymin protein sequence with GGX repeats indicated in yellow.

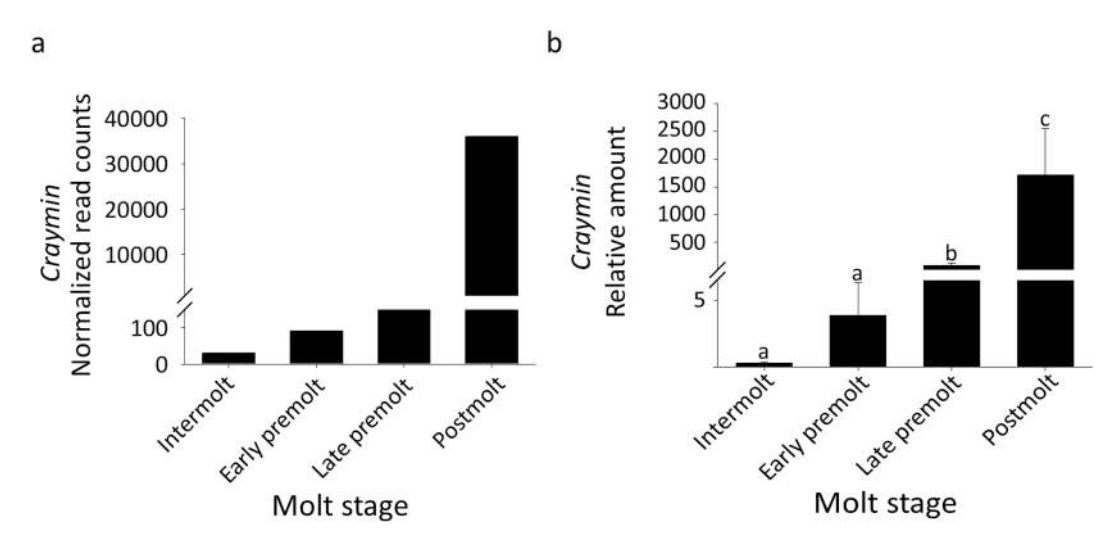


Fig. 2. *In-silico* expression levels and in-vitro validation of *Craymin* molt-related transcription pattern in the cuticle-forming epithelium. a) Transcriptomic library-derived expression pattern of *Craymin* in the four main molt stages (intermolt, early premolt, late premolt, and post molt) of *C. quadricarinatus*. b) Real-time PCR results of *Craymin* in the cuticle-forming epithelium in the four main molt stages. Error bars represent standard error. Different letters indicate statistically significant differences (one-way ANOVA followed by Tukey-HSD post-hoc test; P < 0.05).

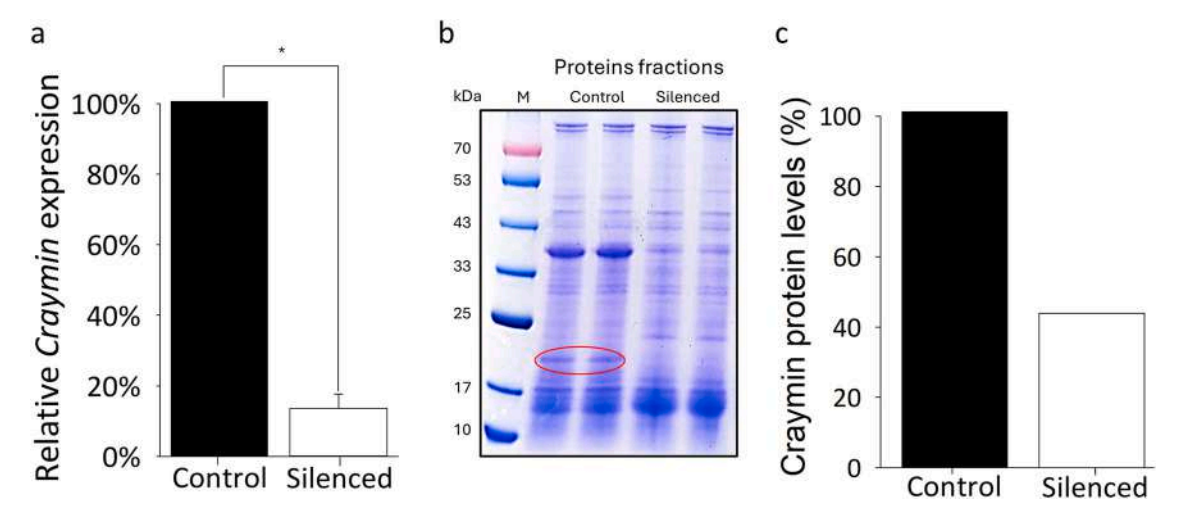


Fig. 3. Craymin silencing efficiency at the transcript and protein levels. a) Relative expression levels following injection of crustacean saline (n = 10) as a control or dsCraymin (n = 10). Error bars represent standard error; asterisk indicates statistically significant difference (P-value <0.05). b) SDS-PAGE gel showing reduction in Craymin protein following knockdown. Craymin protein bands are indicated with a red ellipse. c) Reduction calculation (in percentage, compared to control) following silencing.

3.5. Reduction in cuticular calcium content following Craymin knockdown

Calcium content was determined by EDS, revealing a significant reduction in calcium content following *Craymin* knockdown (Fig. 4). In the control sample, calcium concentrations generally varied from 4.2 %

to >23.3 % (Fig. 4, top panel), but at some points even reached >50 % (Fig. 4, top right panels). In contrast, the *Craymin*-silenced sample showed a significant reduction in calcium concentration, reaching a maximum of approximately 3.5 % (Fig. 4, bottom left panel), thus representing a maximum calcium content reduction of 47 % following Craymin knockdown. Cross-sectional line scans followed the same trend,

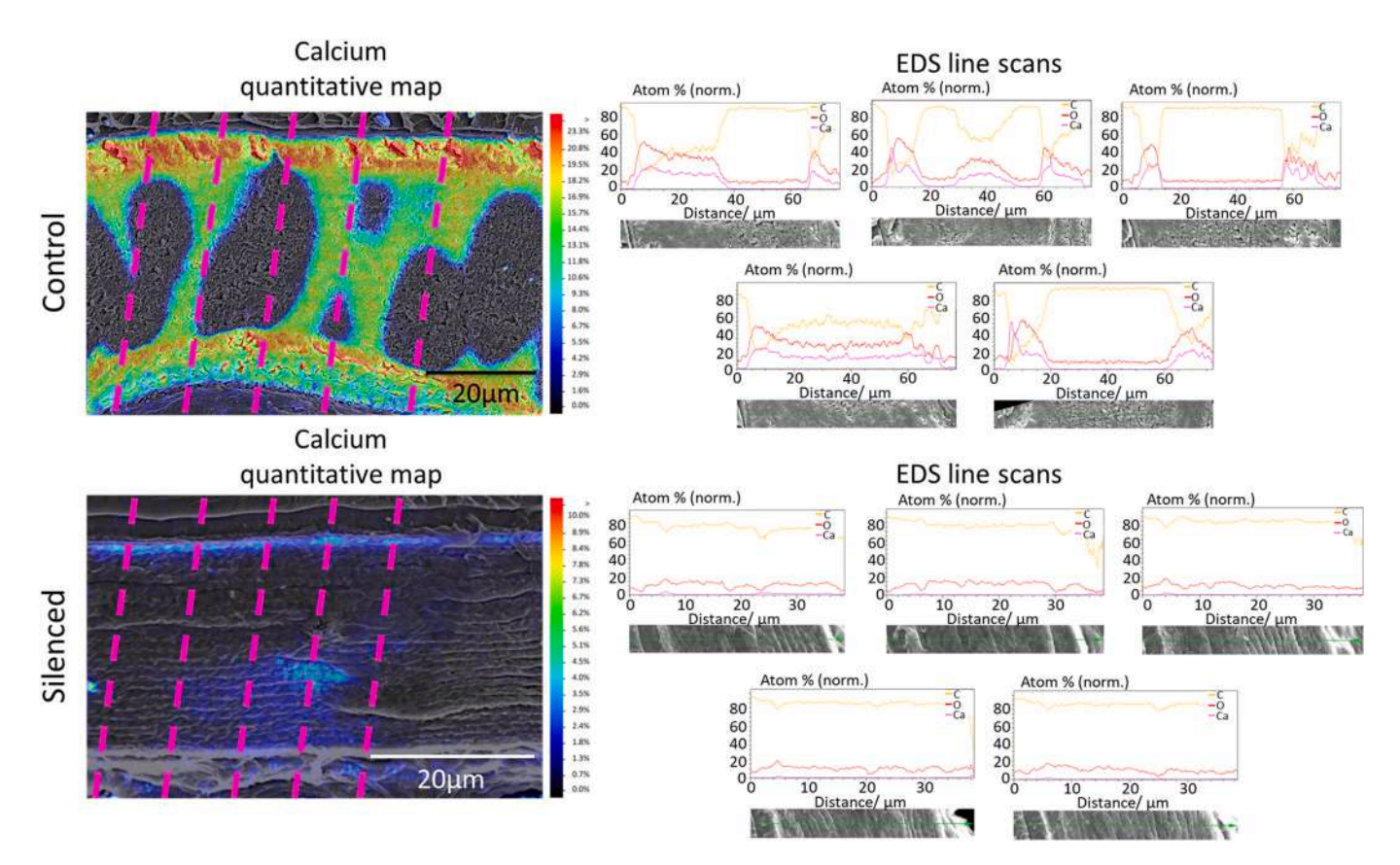


Fig. 4. Cuticle calcium quantification following Craymin knockdown. EDS quantitative maps and line scans of control (top) and silenced (bottom) cuticle cross-sections following Craymin knockdown. The scale bar is 20 μm for the control sample and 13.3 μm for the silenced sample. Calcium concentration is colour coded on the right-hand side of the EDS maps, where red is the highest concentration and black is the lowest. Line scans show changes in carbon (yellow), oxygen (red) and calcium (purple) concentrations across cuticle cross-sections. Locations of the five scanned regions are marked by purple dashed lines on both control and silenced images. Each line scan measurement starts from the top of the respective quantitative map at different locations of the cuticle cross-section.

with the maximum measured calcium concentration in the silenced sample not exceeding 5 % (Fig. 4, bottom right panels). While the EDS spectrum of the control sample (Fig. S5a, left) was comparable to that of the wild-type crayfish [15], the calcium peaks on the EDS spectrum of the treated sample were significantly reduced (Fig. S5a, right). Nonetheless, other representative mineralization-related peaks were not affected in the silenced sample (Fig. S5a, right). In addition, calcium distribution in the control sample (Fig. S5b, left) differed significantly from that in the silenced sample (Fig. S5b, right). Mapping of oxygen and carbon distributions in the silenced sample (Fig. S5c, d, right) revealed marked differences compared to the control sample (Fig. S5c, d, left), indicating that the altered calcium distribution described above was probably a reflection of the presence of CaCO₃ in the cuticular cross section. It is noteworthy that cuticle width also changed, with an average width of approximately 80 µm in the control group (Fig. 4, top left), and almost half that in the Craymin silenced sample (Fig. 4, bottom left). The main layer affected is probably the exocuticle, noted by the significant reduction of the calcium-rich layers seen at the EDS scans following Craymin knockdown (Fig. 4, bottom left) compared to the control sample, demonstrating clear calcium rich layers (Fig. 4, top left).

3.6. Changes in calcium carbonate polymorphs following Craymin knockdown

To determine whether there were changes in the CaCO₃ polymorphs following Craymin knockdown, we used XRD to analyze both the cuticle surface and the most calcium-rich layers identified by quantitative EDS mapping (Fig. 5a, b). XRD revealed significant changes in the CaCO₃ polymorphs following Craymin knock-down. In both control and treated samples, peaks attributed to aragonite and calcite were identified (Fig. 5c). While aragonite is not common in crustaceans exoskeletons, it has been reported before to be present in relatively lower amounts compared to calcite [70,71], thus this finding was not investigated further. The calcite peaks in the control sample were less sharp for diffractograms acquired 2 and 4 µm beneath the surface (Fig. 5c, left, red and blue lines) vs. the corresponding peaks in the silenced cuticular sample (Fig. 5c, right, red and blue lines), implying enhanced calcite crystallization following Craymin knockdown. Rietveld refinement revealed highly crystalline calcite with large crystallites following Craymin knockdown. Calcite crystallite sizes determined by Rietveld refinement were in the nanometer-scale range for the control sample vs. larger than few micrometers (between tens to hundreds micrometers) in the silenced sample (Fig. 5d). Furthermore, full width at half maximum (FWHM) values were significantly higher in the control sample (\approx 5.5), indicating poorly crystallized calcite; in the silenced sample, FWHMs were significantly lower (\approx 0.2), indicating sharper diffraction peaks and higher crystallinity. To confirm these findings, we also analyzed, by XRD, full cuticular cross sections from both the control and silenced samples to determine the main calcium carbonate polymorphs (Fig. S6). Transmission mode spectra acquired for control and silenced samples were similar, with clear peaks attributed to aragonite and calcite (Fig. S6a) being sharper in the silenced sample. Reflectance mode measurements of powdered control and silenced cuticular samples revealed the presence of similar phases (Fig. S6b).

3.7. Cuticle microstructure and ratio between high- and low-rigidity material following Craymin knockdown

To further investigate structural changes in the cuticle following Craymin knockdown, micro-CT scanning was applied (Fig. 6). Density maps revealed a typical cuticle cross section, with a cross-sectional width of \sim 0.1 mm in the control sample (Fig. 6a, left) vs. a significantly thinner cuticle in the silenced sample (0.03 mm; Fig. 6a, right). These results are in keeping with the data acquired from SEM measurements, suggesting that Craymin knockdown interferes with cuticle structural integrity due to decreased mineralization and calcium

dispersion, resulting in fewer hardened cuticular regions. The number of low-density (permeable to X-rays) regions surrounded by high-density (impermeable to X-rays) barriers was reduced by 83 % following *Craymin* knockdown. In keeping with the drop in the in number of low-density regions, the volume of low-density regions and the surface area of their surrounding barriers were markedly reduced in the silenced cuticle by 82 % (Fig. 6b). Following *Craymin* knockdown, the overall reduction in mineralization leads to a significant decrease in calciumrich regions total area.

4. Discussion

Crustaceans are considered one of the most suitable groups of organisms in which to study biological mineral storage and mobilization, as first suggested by Lowenstam and Weiner [1] and subsequently demonstrated in numerous studies [2–7,25,41,72,73]. Due to its distinct and inducible molt cycle, which can be monitored non-invasively [16], together with the availability of a wide molt-related transcriptomic database [29], *C. quadricarinatus* has acquired the status of a leading crustacean for the study of protein-encoding genes involved in exoskeleton formation and mineralization [14,15,27,29,74]. Although several protein-encoding genes involved in exoskeleton formation and mineralization have already been identified, the complete proteinaceous toolkit is far from being revealed, and, in particular, there is a striking lack of knowledge on protein-encoding genes involved in the controlled deposition and crystallization of CaCO₃ in this study animal.

Our preliminary search for proteins involved in the mineralization of the C. quadricarinatus exoskeleton revealed an as-yet unknown glycinerich protein-encoding gene that was significantly expressed during the C. quadricarinatus cuticle mineralization stage. Interestingly, unlike other functional protein-encoding genes involved in such processes, this new candidate gene was not found in other exoskeletal structures, e.g. gastrolith, suggesting its function to be specific to cuticular mineralization. Given the protein's properties, namely, a low molecular weight (17 kDa) and glycine-rich regions encoded by repetitive nucleotide sequences, which are similar to known mineralization-related proteins in other invertebrates [38,45,51], the candidate gene was termed Craymin (crayfish mineralization). Among the glycine-rich proteins in other taxa that are known to be involved in CaCO3 biomineralization [21,38,45,51,75,76], several have G-X and G-G-X repeats that are believed to facilitate protein interaction with calcium at biomineralization sites [49,75-78]. The significantly higher expression levels of Craymin in the cuticle-forming epithelium in the post-molt stage, together with the protein's G-G-X repeats and predicted posttranslational modifications, which facilitate proper protein folding and translocation, suggest that Craymin plays a central role in proper cuticular mineralization. Moreover, the presence of Craymin in both the cuticular and exuvia matrices suggests that it is an integrated structural constituent of the exoskeleton extracellular matrix.

A reduction in Craymin RNA transcripts via RNAi and, therefore, a reduction in Craymin levels, resulted in a significant decrease in exoskeletal calcium levels, suggesting that Craymin is involved in the initial nucleation and sedimentation of biominerals. Similarly, in mollusks, knockdown of a similar glycine-rich protein-encoding gene named Shematrin resulted in reduced CaCO3 crystallization (and thereby decreased shell repair following induced shell breaks) [20,21,37,38,45,79]. Our findings, demonstrating not only calcium reduction but also the formation of larger calcite crystals following Craymin knockdown, suggest similar functions for Craymin and Shematrin. Unlike the oyster shell, where CaCO3 crystals are well ordered and layered [38], the 3D cuticular structure of crustaceans such as C. quadricarinatus is less well ordered, with chitin fibers and different CaCO₃ mineral polymorphs [14] being dispersed throughout the cuticle. Following the discovery that Craymin knockdown resulted in significant calcium reduction in the mineralizing cuticle, however a direct proof of correlation between Craymin presence and calcium distribution could

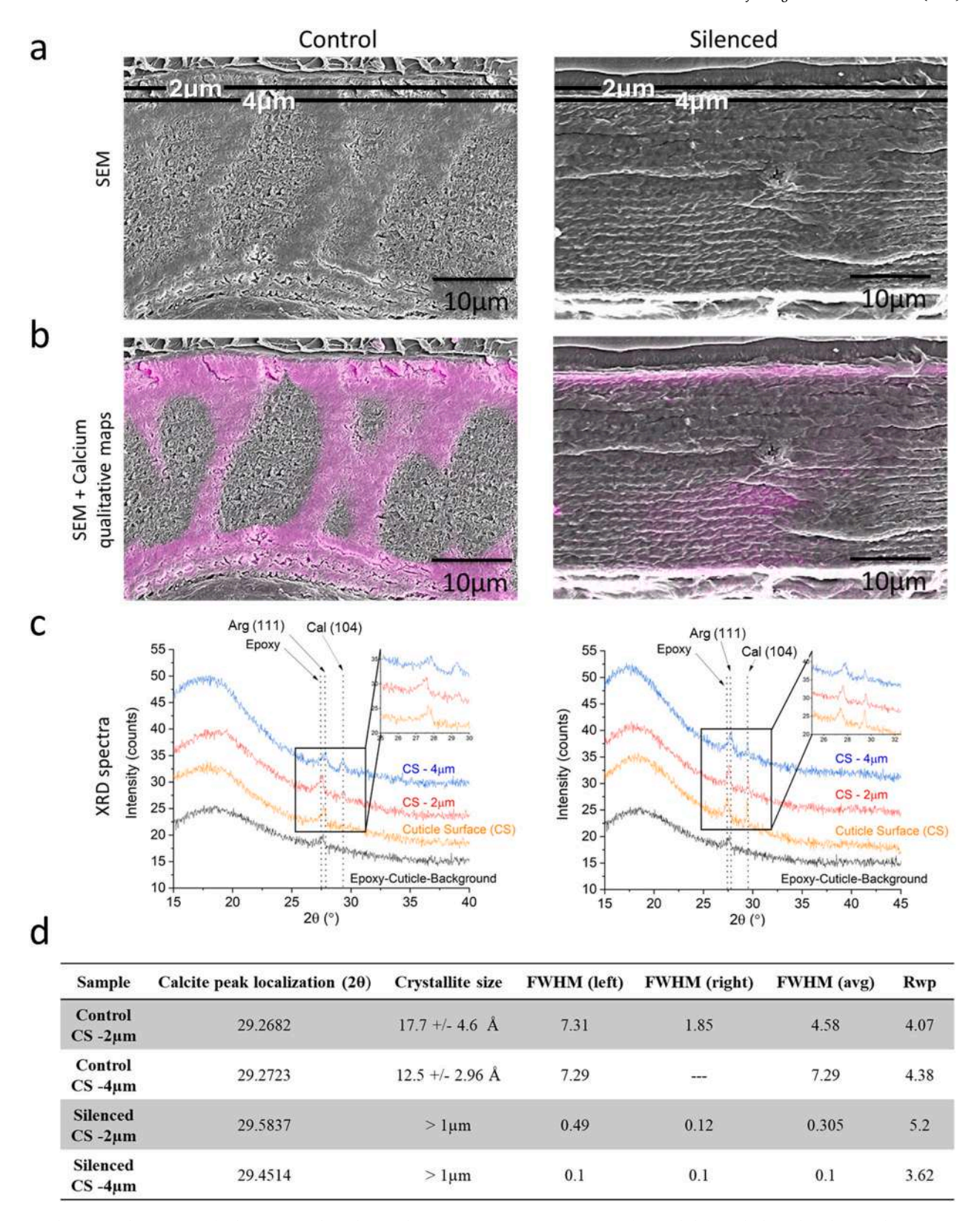


Fig. 5. Localization and properties of calcium minerals in the cuticle. a) Representative SEM images of control (left) and silenced (right) cuticle cross sections. b) Control (left) and silenced (right) SEM images combined with qualitative calcium EDS maps. All scale bars are $10 \mu m$. c) XRD spectra of epoxy background, cuticle surface, and $2 \mu m$ and $4 \mu m$ below the cuticle surface of both control (left) and silenced (right) samples. XRD peaks localization of epoxy, aragonite (Arg), and calcite (Cal) CaCO₃ are noted. Inset images depict changes in aragonite and calcite peaks following Craymin knockdown. d) Interpretation of the XRD spectra following Craymin knockdown. CS – cuticle surface. FWHM – full width at half maximum peak values on the left and right sides for asymmetrical peaks. Avg – average FWHM values. Rwp – weighted profile residual values of fit for the Rietveld refinement model. Locations of XRD scans performed 2 and 4 μ m below the cuticle surface are marked by black lines on both control and silenced SEM images.

а

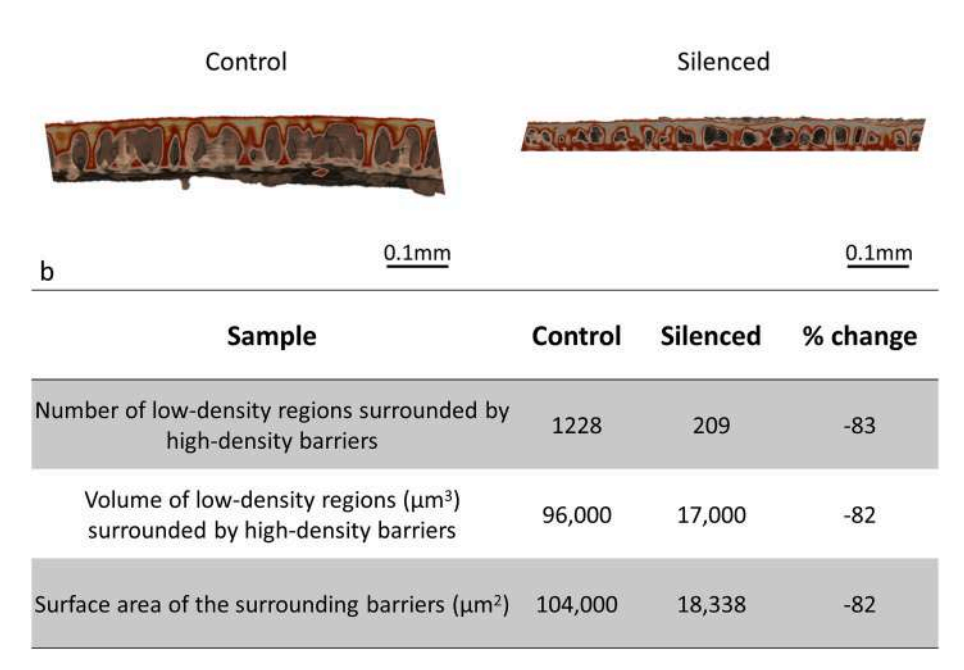


Fig. 6. Cuticle structure and dense material. a) Micro-CT images of control (left) and silenced (right) cuticle samples reveal changes in the distribution of high- and low-density material across the scanned sample. Scale bars are 0.1 mm for all images. b) Table showing the number of low-density (permeable to X-rays) regions surrounded by high-density (non-permeable to X-rays) barriers, their volume, and the surface area of the surrounding barriers, with the corresponding changes in %.

be a future line of research. At any rate, a reduction was also found in the width of the calcium-rich layer compared to that of the control cuticle. This finding suggests a common mechanism of action for Craymin and its counterparts in mineralized biosystems of other organisms, such as mollusks [37] and corals [80]. Similarity could be found even in humans, where glycine-rich proteins are thought to initiate or take part in mineralization, affecting calcium distribution in hardened tissues where collagen serves as a glycine-rich protein scaffold [81,82]. Such findings suggest that glycine-rich proteins like Craymin form a chemically suitable environment for calcium carbonate crystallization, allowing the creation of the required microenvironmental conditions for initial mineral nucleation.

It is noteworthy, that while the most abundant $CaCO_3$ mineral polymorph was calcite (apart from the bulk non crystalline mineral comprising ACC [83]) in both the control and silenced cuticles, crystal size was significantly larger (micrometric) in the silenced sample than in the control (nanometric), despite the overall lower abundance of Ca in the silenced cuticle. This finding suggests a compensation mechanism [32,84–86] to maintain the structural and physical integrity [79] of the silenced cuticle in which large calcite crystals grow to fill in the gaps in the exoskeleton of the silenced animals due to the tempered exoskeletal scaffold. Such phenomena are known and documented in various biomineralization systems, including those of mollusks, echinoderms, and calcareous dinoflagellates [32,84,85].

In keeping with the findings reporting a tempered exoskeleton with larger calcite crystallites, it was intriguing to discover that *Craymin* knockdown also affected cuticular width and structural integrity, indicating that Craymin might reside inside a chitin-associated protein complex and hence affect the chitin-protein-minerals 3D network, as has been previously suggested in crustaceans and other mineralized invertebrates [6,14,49,56,87]. This premise is supported by the micro-CT results showing that *Craymin* knockdown cause a decrease in total surface area of X-ray impermeable barriers within the cuticle. Similarly, other studies have shown that matrix proteins, such as Pif and Shematrin-2, play a crucial role in regulating mineral density and crystallographic orientation in other biomineralizing systems, such as

mollusk shells [22,88]. These findings further strengthen the importance of Craymin in cuticle mineralization and structural integrity, suggesting that it acts as a key protein inside a structural protein complex [6,49,79,87,89] responsible for supporting the shape and size of $CaCO_3$ crystallites in the mineralizing cuticle.

The notion that Craymin is structurally associated with the exoskeletal scaffold was further supported by its presence in protein extracts from cuticle and exuviae exoskeletal scaffolds. Similar proteins were found in other chitin-based biomineralizing organisms [90–93]. Unlike other proteins that are directly associated with chitin [10,68,94–96], Craymin does not possess any of the known chitin-binding domains, and thus its structural association with chitin take place via one of the two already published options in crustaceans [14,68]. First, Craymin could be attached to chitinous structures via its putative glycosylated site, as previously shown for the protein crustacean larval factor in the spiny lobster *Sagmariasus verreauxi* [97]. Second, Craymin could be part of a major protein complex that includes a chitin-binding domain-containing protein, which serves as an anchor to the chitin scaffold, as described in a previously suggested crustacean cuticle model [6,24,27,36,49,89].

In conclusion, this research expands the knowledge on protein-encoding genes involved directly in the sedimentation and polymorphism of $CaCO_3$ minerals in the exoskeletal matrix of the crustacean, C. quadricarinatus. The discovery of Craymin as a structural protein, combined with recent advances in understanding the 3D architecture of crustacean exoskeletons [68], lays down the groundwork for creating advanced biomimetic materials that effectively mimic these natural designs. Such systems are highly promising for tissue engineering processes such as the formation of bone replacement materials.

CRediT authorship contribution statement

Shai A. Shaked: Writing – review & editing, Writing – original draft, Visualization, Validation, Resources, Project administration, Methodology, Investigation, Formal analysis, Data curation, Conceptualization. Rivka Manor: Validation, Methodology, Investigation. Simy Weil:

Validation, Methodology, Investigation, Data curation. Idan Pery: Validation, Investigation. Eliahu D. Aflalo: Validation, Methodology, Investigation. Sana Huleihel: Resources, Methodology, Investigation. Nitzan Maman: Resources, Methodology, Investigation. Lonia Friedlander: Resources, Methodology, Investigation. Amir Sagi: Writing – review & editing, Writing – original draft, Supervision, Funding acquisition, Conceptualization.

Declaration of competing interest

The authors declare that they have no known competing financial interests or personal relationships that could have appeared to influence the work reported in this paper.

Acknowledgements

This research was funded by the Deutsche Forschungsgemeinschaft (DFG, German Research Foundation) – Projektnummer 538923079 (grant KR5132/14-1) and by the Israel Science Foundation (grant 354/18), both awarded to A.S. The authors thank the Dor aquaculture station team and Oran Zimand for the animals used. Dr. Mark Karpasas from the Ilse Katz Institute for Nanoscale Science and Technology, Ben Gurion University of the Negev is thanked for his assistance with MS/MS. Elena Yakub-Ginzburg and Keren Bendalak of the Smoler Proteomics Center at the Technion Israel Institute of Technology are thanked for additional MS/MS analysis.

Appendix A. Supplementary data

Supplementary data to this article can be found online at https://doi.org/10.1016/j.ijbiomac.2025.147911.

Data availability

All the data and supplementary information is available in the main text and in the supplementary information file attached to this submission.

References

- H.A. Lowenstam, S. Weiner, On Biomineralization, Oxford University Press on Demand. 1989.
- [2] H. Inoue, T. Ohira, N. Ozaki, H. Nagasawa, A novel calcium-binding peptide from the cuticle of the crayfish, *Procambarus clarkii*, Biochem. Biophys. Res. Commun. 318 (3) (2004) 649–654.
- [3] D. Raabe, C. Sachs, P. Romano, The crustacean exoskeleton as an example of a structurally and mechanically graded biological nanocomposite material, Acta Mater. 53 (15) (2005) 4281–4292.
- [4] A. Becker, A. Ziegler, M. Epple, The mineral phase in the cuticles of two species of Crustacea consists of magnesium calcite, amorphous calcium carbonate, and amorphous calcium phosphate, Dalton Trans. 10 (2005) 1814–1820.
- [5] D. Raabe, P. Romano, C. Sachs, H. Fabritius, A. Al-Sawalmih, S. Yi, G. Servos, H. G. Hartwig, Microstructure and crystallographic texture of the chitin-protein network in the biological composite material of the exoskeleton of the lobster Homarus americanus, Mat Sci Eng a-Struct 421 (1–2) (2006) 143–153.
- [6] A.V. Kuballa, D.J. Merritt, A. Elizur, Gene expression profiling of cuticular proteins across the moult cycle of the crab *Portunus pelagicus*, BMC Biol. 5 (2007) 1–26.
- [7] A. Shechter, L. Glazer, S. Cheled, E. Mor, S. Weil, A. Berman, S. Bentov, E.D. Aflalo, I. Khalaila, A. Sagi, A gastrolith protein serving a dual role in the formation of an amorphous mineral containing extracellular matrix, Proc. Natl. Acad. Sci. U. S. A. 105 (20) (2008) 7129–7134.
- [8] F. Neues, S. Hild, M. Epple, O. Marti, A. Ziegler, Amorphous and crystalline calcium carbonate distribution in the tergite cuticle of moulting *Porcellio scaber* (Isonoda, Crustacea). J. Struct. Biol. 175 (1) (2011) 10–20.
- [9] H. Nagasawa, The crustacean cuticle: structure, composition and mineralization, Front. Biosci. 4 (2012) 711–720.
- [10] A. Sekimoto, T. Ohira, A. Shigematsu, T. Okumura, M. Mekuchi, K. Toyota, H. Mishima, R. Kawamura, K. Hatano, U. Kawago, Y. Kitani, T. Sekiguchi, T. Amornsakun, J. Hirayama, A. Hattori, H. Matsubara, N. Suzuki, Functional analysis of a matrix peptide involved in calcification of the exoskeleton of the kuruma prawn, Marsupenaeus japonicus, Aquaculture 559 (2022) 738437.
- [11] A. Akiva-Tal, S. Kababya, Y.S. Balazs, L. Glazer, A. Berman, A. Sagi, A. Schmidt, In situ molecular NMR picture of bioavailable calcium stabilized as amorphous

- CaCO3 biomineral in crayfish gastroliths, Proc. Natl. Acad. Sci. U. S. A. 108 (36) (2011) 14763–14768.
- [12] L. Glazer, A. Sagi, On the involvement of proteins in the assembly of the crayfish gastrolith extracellular matrix, Invertebr. Reprod. Dev. 56 (1) (2012) 57–65.
- [13] W.J.E.M. Habraken, A. Masic, L. Bertinetti, A. Al-Sawalmih, L. Glazer, S. Bentov, P. Fratzl, A. Sagi, B. Aichmayer, A. Berman, Layered growth of crayfish gastrolith: about the stability of amorphous calcium carbonate and role of additives, J. Struct. Biol. 189 (1) (2015) 28–36.
- [14] S. Abehsera, S. Zaccai, B. Mittelman, L. Glazer, S. Weil, I. Khalaila, G. Davidov, R. Bitton, R. Zarivach, S.H. Li, F.H. Li, J.H. Xiang, R. Manor, E.D. Aflalo, A. Sagi, CPAP3 proteins in the mineralized cuticle of a decapod crustacean, Sci. Rep. 8 (2018) 2430.
- [15] S.A. Shaked, S. Abehsera, A. Ziegler, S. Bentov, R. Manor, S. Weil, E. Ohana, J. Eichler, E.D. Aflalo, A. Sagi, A transporter that allows phosphate ions to control the polymorph of exoskeletal calcium carbonate biomineralization, Acta Biomater. 178 (2024) 221–232.
- [16] A. Shechter, A. Berman, A. Singer, A. Freiman, M. Grinstein, J. Erez, E.D. Aflalo, A. Sagi, Reciprocal changes in calcification of the gastrolith and cuticle during the molt cycle of the red claw crayfish *Cherax quadricarinatus*, Biol. Bull. 214 (2) (2008) 122–134.
- [17] N. Tsutsui, K. Ishii, Y. Takagi, T. Watanabe, H. Nagasawa, Cloning and expression of a cDNA encoding an insoluble matrix protein in the gastroliths of a crayfish, *Procambarus clarkii*, Zoolog. Sci. 16 (4) (1999) 619–628.
- [18] F. Marin, B. Marie, S.B. Hamada, P. Ramos-Silva, N. Le Roy, N. Guichard, S.E. Wolf, C. Montagnani, C. Joubert, D. Piquemal, Shellome': proteins involved in mollusk shell biomineralization-diversity, functions, Recent advances in pearl research 149 (2013) 168.
- [19] V.B.S. Chan, T. Toyofuku, G. Wetzel, L. Saraf, V. Thiyagarajan, A.S. Mount, Direct deposition of crystalline aragonite in the controlled biomineralization of the calcareous tubeworm, Front. Mar. Sci. 2 (2015).
- [20] J. Liang, J. Xie, J. Gao, C.Q. Xu, Y. Yan, G.C. Jia, L. Xiang, L.P. Xie, R.Q. Zhang, Identification and characterization of the lysine-rich matrix protein family in *Pinctada fucata*: indicative of roles in Shell formation, Marine Biotechnol. 18 (6) (2016) 645–658.
- [21] Y. Chen, J. Gao, J. Xie, J. Liang, G.L. Zheng, L.P. Xie, R.Q. Zhang, Transcriptional regulation of the matrix protein Shematrin-2 during shell formation in pearl oyster, J. Biol. Chem. 293 (46) (2018) 17803–17816.
- [22] X.R. Song, Z.Q. Liu, L.L. Wang, L.S. Song, Recent advances of shell matrix proteins and cellular orchestration in marine molluscan shell biomineralization, Front. Mar. Sci. 6 (2019) 41.
- [23] G. Luquet, F. Marin, Biomineralisations in crustaceans: storage strategies, C. R. Pal. 3 (6-7) (2004) 515-534.
- [24] L. Glazer, A. Shechter, M. Tom, Y. Yudkovski, S. Weil, E.D. Aflalo, R.R. Pamuru, I. Khalaila, S. Bentov, A. Berman, A. Sagi, A protein involved in the assembly of an extracellular calcium storage matrix, J. Biol. Chem. 285 (17) (2010) 12831–12839.
- [25] G. Luquet, Biomineralizations: insights and prospects from crustaceans, Zookeys 176 (2012) 103–121.
- [26] S. Bentov, E.D. Aflalo, J. Tynyakov, L. Glazer, A. Sagi, Calcium phosphate mineralization is widely applied in crustacean mandibles, Sci. Rep. 6 (2016).
- [27] S. Abehsera, S. Weil, R. Manor, A. Sagi, The search for proteins involved in the formation of crustacean cuticular structures, Hydrobiologia 825 (1) (2018) 29–45.
- [28] P. Romano, H. Fabritius, D. Raabe, The exoskeleton of the lobster *Homarus americanus* as an example of a smart anisotropic biological material, Acta Biomater. 3 (3) (2007) 301–309.
- [29] S.A. Shaked, S. Abehsera, T. Levy, V. Chalifa-Caspi, A. Sagi, From sporadic single genes to a broader transcriptomic approach: insights into the formation of the biomineralized exoskeleton in decapod crustaceans, J. Struct. Biol. 212 (2) (2020) 107612.
- [30] K. Alvares, The role of acidic phosphoproteins in biomineralization, Connect. Tissue Res. 55 (1) (2014) 34–40.
- [31] L. Addadi, S. Weiner, Interactions between acidic proteins and crystals stereochemical requirements in biomineralization, Proc. Natl. Acad. Sci. U. S. A. 82 (12) (1985) 4110-4114.
- [32] Y.H. Fang, S.Y. Lee, H.F. Xu, G.A. Farfan, Organic controls over biomineral Ca-Mg carbonate compositions and morphologies, Cryst. Growth Des. 23 (7) (2023) 4872–4882.
- [33] F. Nudelman, Nacre biomineralisation: a review on the mechanisms of crystal nucleation, Semin. Cell Dev. Biol. 46 (2015) 2–10.
- [34] K. Futagawa, Y. Kato, M. Suzuki, Conformational analysis of biomineral proteins interacting with inorganic minerals using dispersive mineral particles for solution NMR, CrystEngComm 27 (14) (2025) 2043–2063.
- [35] C.N. Takacs, J. Hocking, M.T. Cabeen, N.K. Bui, S. Poggio, W. Vollmer, C. Jacobs-Wagner, Growth medium-dependent Glycine incorporation into the peptidoglycan of *Caulobacter crescentus*, PloS One 8 (2) (2013).
- [36] X. Liu, Z. Yin, Z. Ma, J. Liang, L. Yao, R. Zhang, More than 90% of nacre matrix proteins are composed of silk-like proteins, bioRxiv (2022), 2022.09. 07.507049.
- [37] X. Liu, C. Jin, L. Wu, S. Dong, S. Zeng, J. Li, Hic74, a novel alanine and glycine rich matrix protein related to nacreous layer formation in the mollusc *Hyriopsis cumingii*, Aquaculture and Fisheries 2 (3) (2017) 119–123.
- [38] M. Yano, K. Nagai, K. Morimoto, H. Miyamoto, Shematrin: a family of glycine-rich structural proteins in the shell of the pearl oyster *Pinctada fucata* comp, Biochem. Physiol. B, Biochem. Mol. Biol. 144 (2) (2006) 254–262.
- [39] K. Ishii, N. Tsutsui, T. Watanabe, T. Yanagisawa, H. Nagasawa, Solubilization and chemical characterization of an insoluble matrix protein in the gastroliths of a crayfish, *Procambarus clarkii*, Biosci. Biotechnol. Biochem. 62 (2) (1998) 291–296.

- [40] H. Inoue, N. Ozaki, H. Nagasawa, Purification and structural determination of a phosphorylated peptide with anti-calcification and chitin-binding activities in the exoskeleton of the crayfish, Procambarus clarkii, Biosci. Biotechnol. Biochem. 65 (8) (2001) 1840–1848.
- [41] F. Bobelmann, P. Romano, H. Fabritius, D. Raabe, M. Epple, The composition of the exoskeleton of two crustacea: the American lobster *Homarus americanus* and the edible crab *Cancer pagurus*, Thermochim. Acta 463 (1–2) (2007) 65–68.
- [42] G. Luquet, M.S. Fernandez, A. Badou, N. Guichard, N.L. Roy, M. Corneillat, G. Alcaraz, J.L. Arias, Comparative ultrastructure and carbohydrate composition of gastroliths from astacidae, cambaridae and parastacidae freshwater crayfish (crustacea, decapoda), Biomolecules 3 (1) (2012) 18–38.
- [43] B.A. Gotliv, L. Addadi, S. Weiner, Mollusk shell acidic proteins: in search of individual functions, Chembiochem 4 (6) (2003) 522–529.
- [44] Y. Zhang, L.P. Xie, Q.X. Meng, T.M. Jiang, R.L. Pu, L. Chen, R.Q. Zhang, A novel matrix protein participating in the nacre framework formation of pearl oyster, *Pinctada fucata*, Comp. Biochem. Physiol. B Biochem. Mol. Biol. 135 (3) (2003) 565–573.
- [45] B. Marie, G. Luquet, J.P.P. De Barros, N. Guichard, S. Morel, G. Alcaraz, L. Bollache, F. Marin, The shell matrix of the freshwater mussel *Unio pictorum* (Paleoheterodonta, Unionoida), FEBS J. 274 (11) (2007) 2933–2945.
- [46] F. Marin, G. Luquet, Unusually acidic proteins in biomineralization, in: Handbook of Biomineralization: Biological Aspects and Structure Formation, 2007, pp. 273–290.
- [47] M. Wojtas, P. Dobryszycki, A. Ozyhar, Intrinsically disordered proteins in biomineralization, in: Advanced Topics in Biominerlization, 2012, pp. 3–32.
- [48] C. Rivera-Pérez, R.G. Arroyo-Loranca, N.Y. Hernández-Saavedra, An acidic protein, Hf15, from *Hailotis fulgens* involved in biomineralization, Comp. Biochem. Physiol. A 272 (2022)
- [49] C. Liu, W. Zhang, Q. Dong, H. Liu, Exoskeleton protein repertoires in decapod crustaceans revealed distinct biomineralization evolution with molluscs, J. Proteomics 291 (2024) 105046.
- [50] M. Suzuki, E. Murayama, H. Inoue, N. Ozaki, H. Tohse, T. Kogure, H. Nagasawa, Characterization of Prismalin-14, a novel matrix protein from the prismatic layer of the Japanese pearl oyster (*Pinctada fucata*), Biochem. J. 382 (2004) 205–213.
- [51] S. Gayathri, R. Lakshminarayanan, J.C. Weaver, D.E. Morse, R.M. Kini, S. Valiyaveettil, In vitro study of magnesium-calcite biomineralization in the skeletal materials of the seastar *Pisaster giganteus*, Chem. Eur. J. 13 (11) (2007) 3262–3268.
- [52] S. Abehsera, L. Glazer, J. Tynyakov, I. Plaschkes, V. Chalifa-Caspi, I. Khalaila, E. D. Aflalo, A. Sagi, Binary gene expression patterning of the molt cycle: the case of chitin metabolism, PLoS One 10 (6) (2015) e0122602.
- [53] S. Abehsera, S. Peles, J. Tynyakov, S. Bentov, E.D. Aflalo, S.H. Li, F.H. Li, J. H. Xiang, A. Sagi, MARS: a protein family involved in the formation of vertical skeletal elements, J. Struct. Biol. 198 (2) (2017) 92–102.
- [54] H.O. Fabritius, A. Ziegler, M. Friák, S. Nikolov, J. Huber, B.H.M. Seidl, S. Ruangchai, F.I. Alagboso, S. Karsten, J. Lu, A.M. Janus, M. Petrov, L.F. Zhu, P. Hemzalová, S. Hild, D. Raabe, J. Neugebauer, Functional adaptation of crustacean exoskeletal elements through structural and compositional diversity: a combined experimental and theoretical study, Bioinspir. Biomim. 11 (5) (2016) 055006.
- [55] B. Kruppke, J. Farack, S. Weil, E.D. Aflalo, D. Polakova, A. Sagi, T. Hanke, Crayfish hemocyanin on chitin bone substitute scaffolds promotes the proliferation and osteogenic differentiation of human mesenchymal stem cells, J. Biomed. Mater. Res. A 108 (3) (2020) 694–708.
- [56] M. Vittori, Structural diversity of crustacean exoskeletons and its implications for biomimetics, Interface Focus 14 (2) (2024) 20230075.
- [57] E. Gasteiger, C. Hoogland, A. Gattiker, M.R. Wilkins, R.D. Appel, A. Bairoch, Protein Identification and Analysis Tools on the ExPASy Server, 2005, pp. 571–607.
- [58] S.F. Altschul, W. Gish, W. Miller, E.W. Myers, D.J. Lipman, Basic local alignment search tool, J. Mol. Biol. 215 (3) (1990) 403–410.
- [59] F. Sievers, D.G. Higgins, Clustal omega, accurate alignment of very large numbers of sequences, multiple sequence alignment, Methods 1079 (2014) 105–116.
- [60] L. Slabinski, L. Jaroszewski, L. Rychlewski, I.A. Wilson, S.A. Lesley, A. Godzik, XtalPred: a web server for prediction of protein crystallizability, Bioinformatics 23 (24) (2007) 3403–3405.
- [61] A. Untergasser, I. Cutcutache, T. Koressaar, J. Ye, B.C. Faircloth, M. Remm, S. G. Rozen, Primer3–new capabilities and interfaces, Nucleic Acids Res. 40 (15) (2012) e115.
- [62] R. Gupta, S. Brunak, Prediction of glycosylation across the human proteome and the correlation to protein function, in: Biocomputing 2002, World Scientific, 2001, pp. 310–322.
- [63] N. Blom, S. Gammeltoft, S. Brunak, Sequence and structure-based prediction of eukaryotic protein phosphorylation sites, J. Mol. Biol. 294 (5) (1999) 1351–1362.
- [64] C.F.A. Pantin, On the excitation of crustacean muscle. I, J. Exp. Biol. 11 (1) (1934) 11–27.
- [65] T. Levy, S.L. Tamone, R. Manor, E.D. Aflalo, M.Y. Sklarz, V. Chalifa-Caspi, A. Sagi, The IAG-switch and further transcriptomic insights into sexual differentiation of a protandric shrimp, Front. Mar. Sci. 7 (2020) 587454.
- [66] M.D. Abràmoff, P.J. Magalhāes, S.J. Ram, Image processing with ImageJ, Biophotonics Int. 11 (7) (2004) 36–42.
- [67] Z. Roth, S. Parnes, S. Wiel, A. Sagi, N. Zmora, J.S. Chung, I. Khalaila, N-glycan moieties of the crustacean egg yolk protein and their glycosylation sites, Glycoconj. J. 27 (1) (2010) 159–169.
- [68] S.A. Shaked, S. Weil, R. Manor, E.D. Aflalo, S. Moscovitz, N. Maman, R. Maria, B. Kruppke, T. Hanke, J. Eichler, B. Ratzker, M. Sokol, A. Sagi, Cuticular proteins

- (Crusticuls) affect 3D chitin bundle nanostructure, Nanoscale 17 (22) (2025) 13951–13965.
- [69] T. Degen, M. Sadki, E. Bron, U. König, G. Nénert, The highscore suite, Powder Diffract. 29 (S2) (2014) S13–S18.
- [70] S.T. Mergelsberg, R.N. Ulrich, S. Xiao, P.M. Dove, Composition systematics in the exoskeleton of the American lobster, *Homarus americanus* and implications for Malacostraca, Front. Earth Sci. 7 (2019) 69.
- [71] A.M. Fay, A.M. Smith, In a pinch: skeletal carbonate mineralogy of crabs (Arthropoda: Crustacea: Decapoda), Palaeogeogr. Palaeoclimatol. Palaeoecol. 565 (2021) 110219.
- [72] J.H. Tao, D.M. Zhou, Z.S. Zhang, X.R. Xu, R.K. Tang, Magnesium-aspartate-based crystallization switch inspired from shell molt of crustacean, Proc. Natl. Acad. Sci. U. S. A. 106 (52) (2009) 22096–22101.
- [73] A. Sato, S. Nagasaka, K. Furihata, S. Nagata, I. Arai, K. Saruwatari, T. Kogure, S. Sakuda, H. Nagasawa, Glycolytic intermediates induce amorphous calcium carbonate formation in crustaceans, Nat. Chem. Biol. 7 (4) (2011) 197–199.
- [74] S. Abehsera, S. Bentov, X.G. Li, S. Weil, R. Manor, S. Sagi, S.A. Li, F.H. Li, I. Khalaila, E.D. Aflalo, A. Sagi, Genes encoding putative bicarbonate transporters as a missing molecular link between molt and mineralization in crustaceans, Sci. Rep. 11 (1) (2021).
- [75] I. Sarashina, K. Endo, Skeletal matrix proteins of invertebrate animals: comparative analysis of their amino acid sequences, Paleontol. Res. 10 (4) (2006) 311–336.
- [76] H. Endo, Y. Takagi, N. Ozaki, T. Kogure, T. Watanabe, A crustacean Ca²⁺-binding protein with a glutamate-rich sequence promotes CaCO₃ crystallization, Biochem. J. 384 (2004) 159–167.
- [77] A. Al-Sawalmih, C.H. Li, S. Siegel, H. Fabritius, S.B. Yi, D. Raabe, P. Fratzl, O. Paris, Microtexture and chitin/calcite orientation relationship in the mineralized exoskeleton of the American lobster, Adv. Funct. Mater. 18 (20) (2008) 3307–3314
- [78] J. Arivalagan, T. Yarra, B. Marie, V.A. Sleight, E. Duvernois-Berthet, M.S. Clark, A. Marie, S. Berland, Insights from the Shell proteome: biomineralization to adaptation, Mol. Biol. Evol. 34 (1) (2017) 66–77.
- [79] Y. Lin, G. Jia, G. Xu, J. Su, L. Xie, X. Hu, R. Zhang, Cloning and characterization of the shell matrix protein Shematrin in scallop *Chlamys farreri*, Acta Biochim. Biophys. Sin. 46 (8) (2014) 709–719.
- [80] G. Gardella, M.C. Castillo Alvarez, S. Presslee, A.A. Finch, K. Penkman, R. Kroger, M. Clog, N. Allison, Contrasting the effects of aspartic acid and glycine in free amino acid and peptide forms on the growth rate, morphology, composition, and structure of synthetic aragonites, Cryst. Growth Des. 24 (22) (2024) 9379–9390.
- [81] M.D. McKee, B. Hoac, W.N. Addison, N.M. Barros, J.L. Millán, C. Chaussain, Extracellular matrix mineralization in periodontal tissues: noncollagenous matrix proteins, enzymes, and relationship to hypophosphatasia and X-linked hypophosphatemia, Periodontol. 2000 63 (1) (2013) 102–122.
- [82] M.-H. Hong, J.H. Lee, H.S. Jung, H. Shin, H. Shin, Biomineralization of bone tissue: calcium phosphate-based inorganics in collagen fibrillar organic matrices, Biomaterials Research 26 (1) (2022) 42.
- [83] W. Wu, Z. Lu, C. Lu, X. Sun, B. Ni, H. Colfen, R. Xiong, Bioinspired stabilization of amorphous calcium carbonate by carboxylated nanocellulose enables mechanically robust, healable, and sensing biocomposites, ACS Nano 17 (7) (2023) 6664–6674.
- [84] K. Kahil, S. Weiner, L. Addadi, A. Gal, Ion pathways in biomineralization: perspectives on uptake, transport, and deposition of calcium, carbonate, and phosphate, J. Am. Chem. Soc. 143 (50) (2021) 21100–21112.
- [85] A. Picker, M. Kellermeier, J. Seto, D. Gebauer, H. Cölfen, The multiple effects of amino acids on the early stages of calcium carbonate crystallization, Zeitschrift für Kristallographie-Crystalline Materials 227 (11) (2012) 744–757.
- [86] F.J. Li, S. Han, W.J. Chi, X.C. Cui, C.P. Fu, Z.Z. Li, Y. Zhang, J. Liu, A.L. Wang, Identification and functional study of calcification-related peptide from the oriental river prawn, (*Macrobrachium nipponense*), Aquacult. Rep. 27 (2022).
- [87] S. Jasrapuria, C.A. Specht, K.J. Kramer, R.W. Beeman, S. Muthukrishnan, Gene families of Cuticular proteins analogous to Peritrophins (CPAPs) in *Tribolium* castaneum have diverse functions, PloS One 7 (11) (2012).
- [88] M. Suzuki, K. Saruwatari, T. Kogure, Y. Yamamoto, T. Nishimura, T. Kato, H. Nagasawa, An acidic matrix protein, Pif, is a key macromolecule for nacre formation, Science 325 (5946) (2009) 1388–1390.
- [89] S. Jasrapuria, Y. Arakane, G. Osman, K.J. Kramer, R.W. Beeman, S. Muthukrishnan, Genes encoding proteins with peritrophin A-type chitin-binding domains in *Tribolium castaneum* are grouped into three distinct families based on phylogeny, expression and function, Insect Biochem. Mol. Biol. 40 (3) (2010) 214–227.
- [90] S.S. Kumari, D.M. Skinner, Proteins of crustacean exoskeleton: III. Glycoproteins in the Bermuda land crab Gecarcinus lateralis, J. Exp. Zool. 271 (6) (1995) 413–424.
- [91] T.H. Shafer, M.A. McCartney, L.M. Faircloth, Identifying exoskeleton proteins in the blue crab from an expressed sequence tag (EST) library, Integr. Comp. Biol. 46 (6) (2006) 978–990.
- [92] A. Danielli, T.G. Loukeris, M. Lagueux, H.-M. Müller, A. Richman, F.C. Kafatos, A modular chitin-binding protease associated with hemocytes and hemolymph in the mosquito *Anopheles gambiae*, Proc. Natl. Acad. Sci. 97 (13) (2000) 7136–7141.
- [93] N. Raikhel, H. Lee, W. Broekaert, Structure and function of chitin-binding proteins, Annu. Rev. Plant Physiol. Plant Mol. Biol. 44 (1993) 591–615.
- [94] M. Peng, J.C. Cardoso, D.M. Power, Evolution of chitin-synthase in molluscs and their response to ocean acidification, Mol. Phylogenet. Evol. 201 (2024) 108192.

- [95] D. Heymann, H. Mohanram, A. Kumar, C.S. Verma, J. Lescar, A. Miserez, Structure of a consensus chitin-binding domain revealed by solution NMR, J. Struct. Biol. 213 (2) (2021) 107725.
- [96] R.G. Arroyo-Loranca, N.Y. Hernandez-Saavedra, L. Hernandez-Adame, C. Rivera-Perez, Ps19, a novel chitin binding protein from *Pteria sterna* capable to mineralize aragonite plates in vitro, PloS One 15 (3) (2020) e0230431.
- [97] T. Ventura, C. Nguyen, Q.P. Fitzgibbon, T. Abramov, G.G. Smith, A. Elizur, Crustacean larval factor shares structural characteristics with the insect-specific follicle cell protein, Sci. Rep. 9 (2019).